



# G-index: A new metric to describe dynamic refractive index effects in HPLC absorbance detection

Karsten G. Kraiczek<sup>a,c,\*</sup>, Gerard P. Rozing<sup>b,d</sup>, Roland Zengerle<sup>c</sup>

<sup>a</sup> Agilent Technologies, Hewlett-Packard Str. 8, D 76337 Waldbronn, Germany

<sup>b</sup> ROZING.COM Consulting, D 76228 Karlsruhe, Germany

<sup>c</sup> IMTEK – Department of Microsystems Engineering, University of Freiburg, D-79110 Freiburg, Germany

<sup>d</sup> Emeritus Agilent Technologies Research Fellow, 2012, D 76228 Karlsruhe, Germany

## ARTICLE INFO

### Keywords:

Absorbance detection  
Apparent absorbance  
Static and dynamic RI effects  
Gradient elution  
Conventional and liquid core waveguide flow cells  
G-index

## ABSTRACT

High performance liquid chromatography (HPLC) with a solvent gradient and absorbance detection is one of the most widely used methods in analytical chemistry. The observed absorbance baseline is affected by the changes in the refractive index (RI) of the mobile phase. Near the limited of detection, this complicates peak quantitation. The general aspects of these RI-induced apparent absorbance effects are discussed. Two different detectors with fundamentally different optics and flow cell concepts, a variable-wavelength detector equipped with a conventional flow cell and a diode-array detector equipped with a liquid core waveguide flow cell, are compared with respect to their RI behavior. A simple method to separate static – partly unavoidable – RI effects from dynamic RI effects is presented. It is shown that the dynamic RI behavior of an absorbance detector can be well described using a single, relatively easy-to-determine metric called the G-index. The G-index is typically in the order of a few seconds and its sign depends on the optical flow cell concept.

## 1. Introduction

UV–vis spectrophotometric detection has been, and remains, the most frequently used method in (U)HPLC, despite the recent growth in the application of mass spectrometry. Absorbance detectors are considered robust, reliable, easy to use and relatively inexpensive. Today, we look back on a development history of almost exactly half a century.

Two different detector concepts have become established in the market: variable-wavelength detectors (VWD, introduced at the end of the 1960s) and photodiode array-based multiwavelength detectors (DAD, introduced in the early 1980s). In the VWD, monochromatic light selected from a continuous light source is guided through a flow cell and the transmitted light is recorded by a single photodiode. In the DAD, polychromatic light is guided through the flow cell and the transmitted light is guided into a polychromator where a photodiode-array simultaneously records multiwavelength signals [1]. The DAD optics is often referred to as the “reverse optics” to accentuate the difference to the VWD, which came first. The instrumental design of both detector types is governed by limits imposed by the chromatography (HPLC, later UHPLC) that takes place ahead of the detector, more specifically in the HPLC column [2]. The column's physical dimensions: length and diameter, and the particle size of the stationary phase,

determine the required flow rate for optimal performance (efficiency, analysis time) and the volume of the component zones (peaks) eluting from the column. Its thermodynamic properties determine the composition of the solvent (isocratic elution) required to elute the sample components from the column. In practice, the latter also mandates the mobile phase composition to be dynamically modified (increase in solvent strength; gradient elution) during the analysis, since the equilibration constant (or retention factor) of a molecule may easily range over several orders of magnitude.

The solvent delivery system in front of the separation column must be able to comply with requirements dictated by the column properties (flow rate range and composition of the mobile phase, back pressure). Since the solvent eventually delivers the solute zone to the detector, this must be done with a high degree of accuracy and precision of the solvent flow rate and composition to minimize their effects on the overall accuracy and precision of the analysis [3].

In early HPLC, peak volumes were typically 50–150  $\mu\text{L}$  or 10–25 s in base width. HPLC absorbance detectors were equipped with 7–15  $\mu\text{L}$  cells with path lengths typically less than 10 mm and with 0.25 mm i.d. inlet capillaries sufficiently long to allow convenient connection in the HPLC system. Analog electronics with a time constant of 1–2 s was fast enough for adequate registration of the changes in concentration.

\* Corresponding author at: Agilent Technologies, Hewlett-Packard Str. 8, D 76337 Waldbronn, Germany.  
E-mail address: [karsten\\_kraiczek@agilent.com](mailto:karsten_kraiczek@agilent.com) (K.G. Kraiczek).

Typically, these detectors showed a peak-to-peak noise of  $10^{-4}$  absorbance units (AU) and a linear dynamic range of 4 orders of magnitude [4].

The susceptibility to changes in refractive index (RI) was a problem from the beginning of HPLC detector development. RI effects contribute to the noise and drift and affect the shape of the baseline. Increased noise degrades the limit of detection (LOD), and a curved and bumpy baseline complicates the quantitation of peaks near the LOD. Contact of light rays with the inner wall of a cylindrical cell have been identified as a cause of the RI-susceptibility [5]. As the RI changes, some of the light rays that previously reached the photodetector are diverted to the wall and are lost, and light rays that previously were lost to the wall change direction and now reach the photodetector. The refraction of the light rays occurs at the entrance of the cell, at the transition from the quartz window to the liquid, and inside the cell by a so-called ‘liquid lens’ phenomenon [5]. In the mid-1970s, the tapered flow cell was introduced to avoid such wall-contact RI effects [6]. About 15 years later, the formation of a tapered light beam was proposed to avoid light striking the wall of a cylindrical cell [7]. Stewart discussed the design and the performance of optics with regards to RI-susceptibility also considering optical aperture limitations outside the cell [8]. All his optical field and aperture stop considerations are restricted to homogeneous RI conditions in the cell. Reflections at the entrance and exit solvent-window interfaces are described as an unavoidable residual component of *static RI*. Evans and McGuffin [9,10] studied the RI behavior with a ray-tracing model describing the flow cell as a dynamic lens and reported very good agreement with experimental results. The model profiles used consider radial and axial differences in RI. The calculated *dynamic RI* agreed in direction, shape and magnitude with the measurement results.

Burin et al. [11] studied RI effects in straight and curved or angled fused-silica capillary-based cells. It was found that Z- and U-shaped, longitudinally-illuminated cells had a higher susceptibility to RI than straight, transversely illuminated cells and thus lost part of their path-length advantages. Renn and Synovec [12] reported a quite different approach to absorbance detection. Their multiwavelength absorbance detector using a position-sensitive detection device offered a useful reduction of the RI-effects. Other investigations into different approaches to absorbance detection, such as the LED-based absorbance detector with a reflective cell and the capillary-scale light-emitting-diode-based multi-reflection absorbance detector also included a consideration of RI-effects [13,14].

Continuing efforts in the development of HPLC instrumentation, for example, in the optics of spectrophotometric detectors, digital electronics, signal processing and thermal design, have led to the achievement of noise levels below 10  $\mu$ AU. Unfortunately, the reduced baseline noise now makes RI effects even more apparent.

Modern (U)HPLC systems, however, deliver peaks with volumes and time-based widths 10–50 times smaller than those obtained previously. Consequently, the volume of the cell must be small to conserve the fidelity of the profile of the component zone eluting from such modern (U)HPLC columns. However, the path length still must be long enough for sufficient detection sensitivity. The requirements of small volume and long path length represents a conflict, and a compromise needs to be reached that provides adequate signal-to-noise ratio (SNR) with an acceptable loss in resolution for the chromatography [15].

Traditional (non-waveguide) flow cells are still widely used and are typically either cylindrical or conical. Both geometries share the same volume-to-length relation for the light conductivity (or light throughput). The light conductivity of the cell is proportional to the square of the volume and inversely with the fourth power of the path length [15,16]. For this reason, the path length of traditional cells is usually limited to a maximum of 10 mm.

In recent years, the advent of liquid core waveguide (LCW) cells has made possible high sensitivity, long-path-length detector cells with small volumes. LCW cells are also easy to couple to light sources and

photodetectors [17]. Because of their unique properties, LCW cells are increasingly replacing traditional cells in spectrophotometric HPLC detection; however, the fundamental resolution/SNR dilemma remains unchanged [15].

In this paper we want to review the general aspects of apparent absorbance related to RI in spectrophotometric HPLC detection, and to expand these considerations to modern LCW cells. We introduce a new metric, the G-index, that allows a quantitative description of the dynamic RI behavior of HPLC absorbance detectors.

## 2. Baseline noise

Any fluctuation of the intensity signal that is not related to absorbance of the analyte, for example, noise or drift is undesirable and must be minimized. There are fundamental and technical limitations. Shot-noise is a fundamental limitation. Shot-noise expressed in absorbance units is inversely proportional to the square root of the measured intensity (of the measured photocurrent). The available photon flux for a typical HPLC absorbance detector that is converted into a photocurrent is in the order of  $10^{11}$  to  $10^{12}$  photons per second at an optical bandwidth of 4 nm. Peak-to-peak noise values better than, e.g.,  $10^{-5}$  to a few  $10^{-6}$  AU at a response time of 1 s are not possible due to shot-noise limitations. Such noise levels can be measured with today's HPLC absorbance detectors under moderate flow or stop-flow conditions. Technical limitations include electronic-noise, flicker-noise of the light source and RI-related noise. Electronic-noise is negligible near zero absorbance and flicker-noise becomes visible at only relatively high photocurrents when shot-noise is no longer the limit.

As a component of the optics, the detector flow cell behaves as a living optical element. Any change in the RI distribution in the cell that falls in the noise bandwidth of the detector may result in RI-noise and increase the overall noise of the detector. The long list of factors influencing RI-noise includes flow cell configuration and geometry, detector optics, flow rate and flow stability, solvents, temperature, changes in temperature difference between the solvent and the cell as the specific heat capacity of the eluent changes [8,18], incomplete mixing, gradient elution, gradient slope, ... turbulences in the cell occurring at a certain Reynolds number [19], etc. Stewart concluded that the same optical solutions that are used to minimize the RI-susceptibility to gross RI changes can also be applied to the reduction of RI-noise [18]. Heat exchangers, either directly in front of the cell or integrated into it to reduce the temperature difference between the solvent and the cell are proven measures. In LCW cells, wall reflection is integral to waveguiding, and not all rules for traditional cells apply. Unlike shot-noise, RI-noise is theoretically difficult to predict because the exact RI distribution in the cell at any moment in time would have to be known.

## 3. Apparent absorbance due to changes in Fresnel losses

Absorbance is measured as the log ratio of two intensities.

$$A_t = \log \frac{I}{I_0} = \log \frac{I_0}{I_t} \quad (1)$$

Refractive index effects not only affect the optical path of light rays and thereby contribute to noise but also have a direct effect on the measured intensity level and thus on the absorbance signal. When light rays pass through the detector flow cell, reflection losses occur at the solvent-window interfaces. Because of the relatively low angle of incidence, the reflection losses  $R$  at each window can be calculated accurately enough using the Fresnel equation for the case of normal incidence:

$$R = \left( \frac{n_q - n_s}{n_q + n_s} \right)^2 \quad (2)$$

where  $n_q$  and  $n_s$  respectively connote the RI of quartz and the solvent. For the magnitude of the reflection losses, e.g., quartz window/water  $R = 0.35\%$ , multiple reflections need not be considered. The effective absorbance change  $A_F$  for the two solvent-window interfaces from Fresnel losses is given by:

$$A_F = 2 \cdot [\log(1-R_0) - \log(1-R_s)] \quad (3)$$

where  $R_0$  is the reflection loss with the solvent at balance ( $t = 0$ ) and  $R_s$  is the reflection loss with the solvent at time  $t$ . Eq. (3) directly calculates the effective absorbance change due to RI change and describes only the Fresnel losses, the unavoidable component of the *static* RI, at homogeneous refractive index in the cell. The susceptibility of the measured absorbance to RI changes of the solvent ( $dn/dn$ ) is substantial and typically about  $-0.04$  AU/RIU. In the case of gradient elution, the RI of the solvent can change easily in the  $10^{-3}$  RIU range. RI-effects in the  $10^{-4}$  AU range are to be expected and will be clearly visible at a detector noise of  $10^{-5}$  AU. The temperature coefficients of RI for solvents ( $dn/dT$ ) are relatively high and different, e.g.,  $1 \cdot 10^{-4} \text{ K}^{-1}$  for water and  $4 \cdot 10^{-4} \text{ K}^{-1}$  for methanol. The curvature of a baseline in gradient elution may well change with temperature in the  $10^{-4}$  AU range.

### 3.1. Water – methanol gradient

One of us measured the refractive index of water / methanol mixtures in steps of 5% at 3 temperatures (25 °C, 35 °C, 45 °C) and 3 wavelengths (435 nm, 546 nm, 576 nm) in 1983. These measurement data are quite comparable with the data found in the literature [20–23].

Fig. 1 shows the RI of water – methanol mixture as a function of the methanol concentration. First the RI increases with increasing methanol concentration, reaching a maximum at about 50%. Then the RI falls increasingly as pure methanol is approached. Refractive index equality to pure water is at approximately 83%. The measured curves  $n = f$  (methanol concentration) are easy to fit with polynomials at very good quality;  $r^2$  for fit  $> 0.996$  for polynomial of 5th order. Extrapolation to shorter wavelengths using common dispersion formulas of Hartmann or Schott or Cauchy was found not to be necessary because all later observations clearly show that the relative RI curve is the same even at 250 nm. Nevertheless, the lower the wavelength, the higher the RI. The RI difference with respect to the quartz window at shorter wavelengths, however, remains essentially the same because the RI of quartz is also greater at a lower wavelength [24].

With a water-methanol gradient, the reflection losses decrease with increasing methanol concentration because the RI difference to the quartz window decreases. This results in an increased transmission and leads to negative absorbance. A minimum is reached near 50%, when the RI difference to the quartz window is lowest. The zero-crossing (RI equality with pure water) depends on the temperature and is between 77% (45 °C) and 89% (25 °C). The highest transmission loss is where the difference in RI is largest, with pure methanol (Fig. 2).

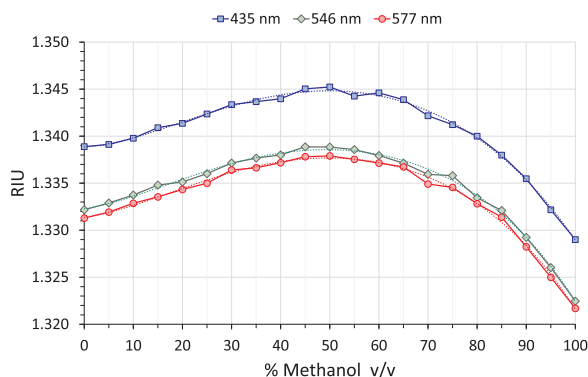


Fig. 1. Refractive index of water – methanol mixture measured at 3 wavelengths. Data shown are for  $T = 35$  °C.

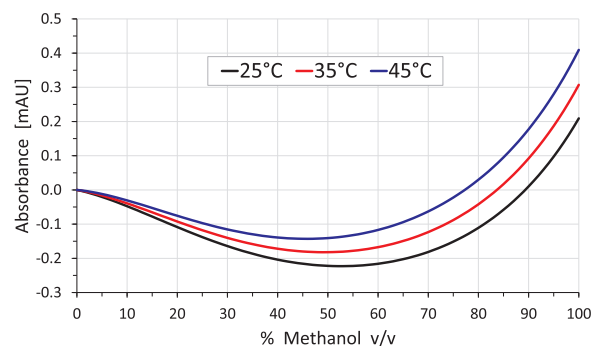


Fig. 2. Apparent absorbance due to changes in Fresnel losses calculated with Eq. (3) using 5th order polynomial fitted RI data measured at 546 nm (25 °C, 35 °C, 45 °C). The curves shown are typical in shape and magnitude for the visible as well as for the UV range.

The difference in RI between the inlet and outlet of the cell in gradient mode depends on the flowrate, the cell volume, the gradient slope and the solvent mixture used. In the case of water-methanol at a flow rate of 1 mL/min, a cell volume of 13  $\mu\text{L}$  and a gradient slope of  $+10\%$ /min, the RI difference can range between  $+2 \cdot 10^{-5}$  at 20% methanol and  $-1 \cdot 10^{-4}$  near 100% methanol. Such differences are not negligible in the context of dynamic RI effects but are negligible in terms of changes in Fresnel losses.

### 3.2. Numerical aperture of LCW flow cell

The light conductivity of LCW flow cells is proportional to the square of its (effective) numerical aperture ( $NA_{LCW}$ ) which in turn is defined by Eq. (4):

$$NA_{LCW}^2 = n_s^2 - n_{clad}^2 \quad (4)$$

where  $n_s$  and  $n_{clad}$  respectively connote the RI of the solvent and the media at which total internal reflection occurs. The wall material RI does not change. As such, without appropriate measures, any changes in solvent RI will profoundly affect the overall transmission through the flow cell, especially in the gradient mode. This is particularly true for LCW flow cell designs where the difference in RI between the solvent and the cladding is small. Potential apparent absorbance changes due to NA-RI changes are calculated using the following equation:

$$A_{NA-RI} = 2 \cdot \log \frac{NA(t=0)}{NA(t)} \quad (5)$$

Two kinds of LCW designs are commonly used in HPLC absorbance detection. Type-I designs are true LCWs, where total internal reflection occurs at the interface between the liquid and a wall material of lower refractive index. In type-II designs, total internal reflection occurs at the external surface of a transparent wall material confining the liquid [25,26]. In the water-methanol example the potential apparent absorbance caused by changes in RI for a type-I Teflon AF-based [17,27] LCW cell ( $n_{clad} = 1.29$ ) that is not limited in its NA by design can be as high as  $-30$  mAU at 50% methanol and  $+54$  mAU at pure methanol. For a type-II fused-silica capillary-based LCW cell where total reflection occurs against air the effect is about  $-8$  mAU or  $+13$  mAU. The susceptibility to RI changes for an FS capillary-based LCW is lower than that for Teflon AF. However, the degree of potential baseline deformations of both cell types is too high to be acceptable in sensitive HPLC applications and involve increased risk of RI-induced noise. Therefore, LCW cells for HPLC detectors are deliberately limited in their numerical aperture by other components of the optics, e.g., when an optical fiber is used to couple light in the cell or optical fibers are used to couple the light both in and out of the cell. For example, the numerical aperture of optical fibers for the UV is about 0.22 and well below the numerical apertures of either of the above-mentioned LCW cell types.

## 4. Experimental section

### 4.1. HPLC system, solvents and methods

The HPLC system consisted of a G1322A Vacuum Degasser, G1312B 1260 Binary Pump, G1316 1260 Temperature-Controlled Column Compartment, G4212B 1260 Diode-Array Detector (DAD), G1314F Variable-Wavelength Detector (VWD). SST capillaries 0.17 id to connect the various modules of the system. Methanol: LiChrosolv gradient grade for LC from Merck. Water was prepared using the Water Purification System Milli-Q Integral 3 from Millipore. The detectors were always connected in series, DAD first, then VWD. The output of both detectors was recorded at 10 Hz, detector rise time 1 s. The flow rate was 1 mL/min unless specified otherwise in the text. Temperature of the Column Compartment was 35 °C unless specified otherwise in the text. Baseline experiments were carried out without a column.

### 4.2. Flow cells

The DAD was equipped with the G4212A Max-Light Cartridge Cell (part number G4212-60008). Cell volume is 2.5  $\mu$ L, path length is 10 mm. The flow cell is a cylindrical type-II capillary LCW [26,28]. The VWD was equipped with the G1314-60186 flow cell. Cell volume is 13  $\mu$ L, path length is 10 mm. The flow cell geometry is conical with a taper angle of  $\pm 3.5^\circ$ .

## 5. Results and discussions

### 5.1. Baseline experiments

Fig. 3 shows water-methanol gradients for the DAD and VWD at 250 nm. Both detectors were connected in series. The DAD came first (blue traces), then the VWD (red traces). The flow rate was 1 mL/min. The solvent composition was changed continuously from 5% to 95% methanol, starting at  $t = 5$  min at a rate of + 10%/min. After 5 min of 95% methanol, the gradient was reversed and ramped down to 5% methanol at a rate of - 10%/min. The peak-to-peak noise of both detectors is better than  $10^{-5}$  AU.

Both detectors measure the same plateau height; + 2.9 mAU (traces labeled with a)). Under stable experimental conditions, typically after 2–3 blank runs, the baseline reproducibility is better than 5%. In the UV, the RI effects are superimposed on the background absorbance of

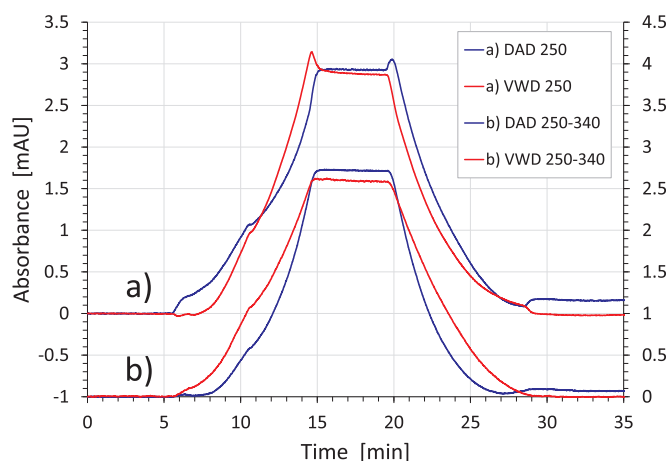


Fig. 3. Water-methanol gradient 5–95%–5% at 250 nm. Solvent temperature = 35 °C. Blue traces: DAD with LCW cell. Red traces: VWD with tapered cell. a) no optical reference. b) DAD with 'online' optical reference and VWD with offline correction (Run 250 nm – Run 340 nm). (For interpretation of the references to color in this figure legend, the reader is referred to the web version of this article.).

the methanol. The curvature in the ascent and descent is mainly due to RI (compare with Fig. 2). The background absorbance of methanol depends, of course, on the wavelength and on the concentration of dissolved gases [29]. A 1% change in oxygen level can cause a 4 mAU change at 210 nm and still a 0.16 mAU change at 250 nm [30,31]. Changes in the oxygen level can cause drift in the UV signal.

The time delay for the composition change to arrive at the detectors was about 0.5 min. At 6.5 min and 10.5 min, small humps are visible in the upslope of the gradient that can be attributed to a contamination in the methanol that was not investigated further. These humps are true UV absorbance and are seen clearly by both detectors. In a practical case it will be obvious that such a peak near the limit of detection is more difficult to quantitate under this condition.

At the isocratic/gradient and gradient/isocratic transition points, the DAD and the VWD respond differently. For example, at 5.5 min the DAD responds with an increase in the signal while the VWD responds with a decrease in the signal. The expected curvature due to changes in Fresnel losses in the gradient profile is better seen on the falling side than on the rising side. Both detectors reach the zero absorbance value not immediately at the end of the inverse gradient but at 40 min (not shown).

In a VWD, the reference signal is picked up in front of the cell and is of the same wavelength. This can compensate for fluctuations in intensity of the light source but not for RI effects in the cell. In a DAD, the light for the optical reference shares essentially the same optical path through the cell but is of a different wavelength. The advantage here is that common baseline effects in the optical flow path can be compensated for (see traces labeled with 'b' where the overshoots have disappeared).

What is true AU and what is RI? How can the overshoots be explained and why are they different?

To answer these questions, the effects from AU and RI must be consistently separated, and the wavelength must be chosen such that the background absorbance of methanol is small relative to RI effects, e.g., at 340 nm.

Fig. 4 shows the same water-methanol gradient measured at 340 nm under otherwise identical conditions. Compare with Fig. 3. The comparison with the calculation shows that a substantial portion of the static RI is due to unavoidable changes in Fresnel losses. In other words, the deviation from Fresnel is primarily due to dynamic RI effects.

Next, the dynamic RI effects are separated from the static RI effects. For this purpose, the continuous gradient is divided into sub-sections of 5%, each having the same slope as the continuous gradient: + 10%/

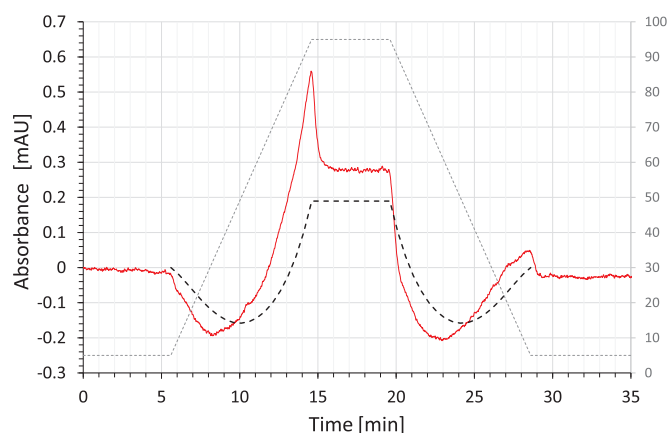
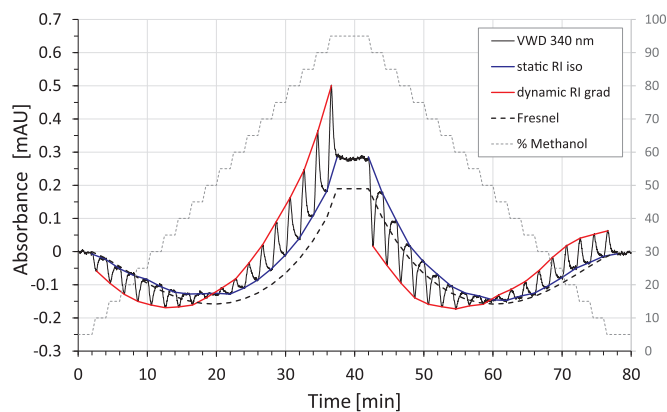


Fig. 4. Water-methanol gradient 5–95%–5% VWD at 340 nm. Solvent temperature = 35 °C. Red trace: VWD. Black dashed trace: expected apparent absorbance due to changes in Fresnel losses calculated using Eq. (3). Gray dashed trace with secondary scale: methanol concentration. (For interpretation of the references to color in this figure legend, the reader is referred to the web version of this article.).



**Fig. 5.** Water-methanol slope/step gradient 5–95%–5% VWD at 340 nm. Solvent temperature = 35 °C. Black trace: measured detector response. Red trace: connection line for dynamic RI. Blue trace: connection line for static RI isocratic. Black dashed trace: expected apparent absorbance due to changes in Fresnel losses calculated using Eq. (3). Gray dashed trace with secondary scale: methanol concentration. (For interpretation of the references to color in this figure legend, the reader is referred to the web version of this article.)

min for the upslope and  $-10\%/min$  for the downslope. Before and after each 5% sub-gradient, an isocratic section is added to capture the static RI portion.

The separation of the dynamic and the isocratic static RI can be clearly seen in Fig. 5. The red connecting line of the dynamic “RI peaks” corresponds to the continuous gradient curve shown in Fig. 4. The blue connecting line of the short isocratic baseline sections highlights the static RI for the given flow conditions. The static RI under isocratic conditions can be explained to a large extent by changes in Fresnel losses. The remaining difference increases linearly with the methanol concentration and may be related to a residual background absorbance of the methanol at 340 nm. This is not significant for this discussion and was not further investigated. In cases where the temperatures of the cell and the solvent are significantly different, the experiment can be extended with stop-flow sections to further differentiate pure Fresnel from isocratic static RI. While up-slope and down-slope for the dynamic RI are quite different (red trace), the isocratic static RI for up- and down-slope match very well (blue trace).

As soon as the concentration change arrives in the cell, a dynamic lens immediately forms — as postulated by Evans and McGuffin [9,10] — resulting in dynamic “RI peaks”. In a reverse-flow experiment (inlet and outlet of cell exchanged), the direction of the dynamic RI-peaks did not change, a result that is at variance with the Evans and McGuffin dynamic lens model.

## 5.2. Separating dynamic and static RI for the DAD with LCW cell

The response of the DAD, which was connected in series with the VWD, was recorded for the same water-methanol gradients. See Figs. 6 and 7. Several important observations can be made. For the LCW cell, the picture is almost exactly the opposite of the VWD case: positive curvature for DAD, negative curvature for VWD. The red connecting line of the dynamic “RI peaks” in Fig. 7 corresponds to the continuous gradient curve shown in Fig. 6. The blue connecting line of the short isocratic baseline sections highlight the isocratic static RI. However, the isocratic static RI does not match the RI effects expected by the Fresnel losses. Reversing the flow does not reverse the static RI effect and does not change the direction of the dynamic RI effect.

Ray tracing of the present LCW design explains the small effect in the magnitude and direction of the static RI, which is related to the length of the LCW cell. A longer path length cell, e.g., 60 mm, of otherwise the same geometry, has a negative curvature.

The transmission characteristic of an optical fiber coupled LCW cell

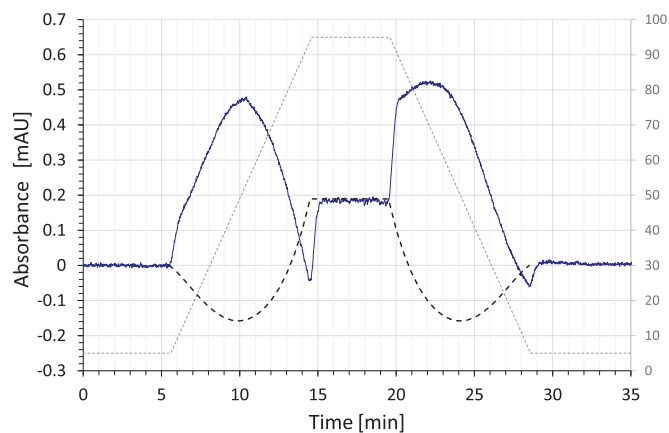


**Fig. 6.** Water-methanol gradient 5–95%–5% DAD at 340 nm. Solvent temperature = 35 °C. Blue trace: DAD. Black dashed trace: expected apparent absorbance due to Fresnel losses calculated using Eq. (3). Gray dashed trace with secondary scale: methanol concentration. (For interpretation of the references to color in this figure legend, the reader is referred to the web version of this article.)

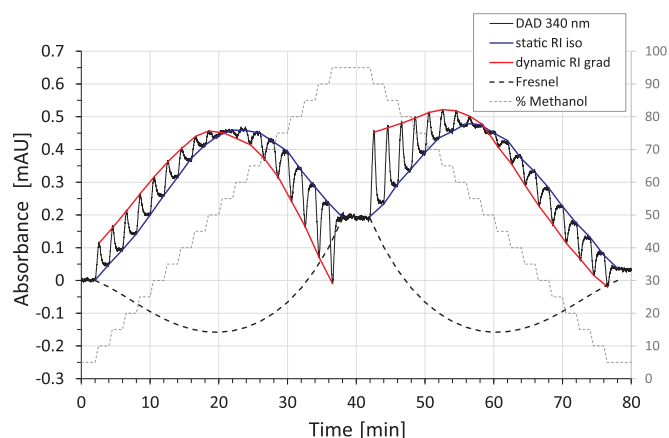


**Fig. 7.** Water-methanol slope/step gradient 5–95%–5% DAD at 340 nm. Solvent temperature = 35 °C. Black trace measured detector response. Red trace: connection line for dynamic RI. Blue trace: static RI isocratic. Black dashed trace: expected apparent absorbance due to changes in Fresnel losses calculated using Eq. (3). Gray dashed with secondary scale: methanol concentration. (For interpretation of the references to color in this figure legend, the reader is referred to the web version of this article.)

is a damped oscillating function [25] along the optical axis, irrespective of the type (type-I or type-II). It takes some distance for the intensity distribution within the flow cell to stabilize in the transverse direction. Meaningful LCW cell designs have a length-to-diameter ratio  $> 10$  to develop a waveguide zone. With increasing distance, the intensity and angular distribution of the light at the inlet of the cell is better mixed. This is particularly true for a type-II LCW, where the light ray splits with every contact with the inner wall into a fraction that is reflected and one that is further transmitted to the external surface where total internal reflection occurs. One source (or parent) ray can split into many thousands of child rays, resulting in very efficient light mixing within the LCW cell. With a change in RI, the oscillating transmission curve experiences a small phase shift resulting also in a change of the transverse intensity distribution in the exit plane of the cell, where the output fiber collects the light. In the design investigated in this study, this results in a positive curvature of the static RI for a 10 mm LCW cell and a negative curvature for a 60 mm LCW cell. At this point, it must be emphasized that the magnitude of the static RI curvature is only a few tenths of a mAU; this is the same magnitude as changes in Fresnel losses

and is small relative to typical chromatographic peak heights.

The direction of the dynamic RI is maintained with increasing path length. The height of the dynamic RI-peaks increases with path-length; however, the increase in detection sensitivity due to path-length according to Lambert-Beer's law dominates.

### 5.3. G-index for an absorbance detector

The height of the “dynamic RI-peak” is proportional to the slope of the refractive index time curve.

$$A_{RI_{dyn}}(t) = G \cdot \frac{dn}{dt} \quad (6)$$

If  $dn/dt$  is known, the proportionality factor  $G$  can be calculated from the height  $A_{RI_{dyn}}$  of the dynamic RI peak.  $G$  can serve as a quality index for the RI-susceptibility of an HPLC detector. The unit of  $G$  is [s] but could also be expressed as AU·s/RIU to better describe the characteristics of  $G$ . However, in this work we use the shorter form [s]. In the following,  $G$  is designated as the “G-index”. It is more convenient to determine the G-index using the area under the dynamic RI-peak,  $Area_{RI_{dyn}}$ . This method of determining the G-index requires only the knowledge of the RI difference  $\Delta n$ .

$$\int_{t_1}^{t_2} A_{RI_{dyn}}(t) \cdot dt = G \cdot \int_{n_1}^{n_2} dn \quad (7)$$

$$Area_{RI_{dyn}} = G \cdot [n_2 - n_1] = G \cdot \Delta n \quad (8)$$

According to Eq. (8), the area under the “dynamic RI-peak” is proportional to the RI difference and is not dependent on the gradient speed.

The G-index evaluation of the slope/step gradients for the VWD and DAD shown in Figs. 5 and 7 is summarized in Table 1. In the gradient from water to methanol, slightly higher G-indices were determined than in the reverse gradient, from methanol to water. The G-index was calculated from the slope of a linear regression using the dynamic RI height and area method. All 36 RI peaks have been processed;  $r^2$  for all fits > 0.97.

In the next experiment, designed to prove that  $Area_{RI_{dyn}}$  is independent of the slope of the gradient,  $\Delta n$  is kept constant but the gradient slope is changed. The methanol concentration is switched back and forth between 25% B and 30% B at different gradient slopes:  $\pm 2.5\%/min$ ,  $\pm 5\%/min$ ,  $\pm 10\%/min$ ,  $\pm 20\%/min$ .

Fig. 8 shows the experimental run for the VWD and DAD at 250 nm. The average area under the dynamic RI peaks is fairly constant for both detectors; mean  $\pm$  standard deviation for the area being, e.g., for the VWD  $[2.16] \pm 0.12$  mAU·s. The RI difference  $|\Delta n| = 8.26 \cdot 10^{-4}$ . This results in a G-index for the VWD of  $-2.62 \pm 0.15$  s at 250 nm and corresponds very well to the result at 340 nm (Table 1). The G-index for the DAD from area is  $+3.21 \pm 0.30$  s; slightly higher than that measured at 340 nm. The evaluation using the dynamic RI height method is, in this example, more difficult because the height is not easy to determine, and results in a higher standard deviation. A G-index of  $-2.52 \pm 0.88$  s was determined for the VWD using the height method, the G-index for the DAD by the same method was  $+2.97 \pm 0.90$  s. Note: In both calculation methods, attention must be paid to the signs for the area, height and  $\Delta n$  to get the correct sign for the G-index. The fact that, with the DAD, the dynamic RI effects are well compensated using optical referencing suggests that the wavelength-dependence of the G-index for the DAD is also not particularly great.

**Table 1**  
G-index at 340 nm for VWD (traditional cell) and DAD (LCW cell).

340 nm	Height	Area
VWD	- 2.57 s	- 2.60 s
DAD	+ 2.49 s	+ 2.84 s

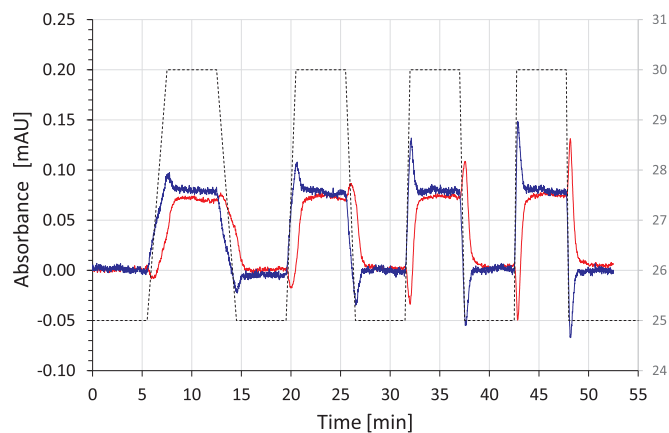


**Fig. 8.** Water-methanol sub-gradients 25%–30% at different gradient slopes. Red trace: VWD at 250 nm. Blue trace DAD 250 nm. Solvent temperature = 35 °C. Gray dashed with secondary scale: methanol concentration. (For interpretation of the references to color in this figure legend, the reader is referred to the web version of this article.)

While the importance of the G-index should not be overstated, it is still amazing how a single metric,  $G$ , allows a good qualitative prediction of the gradient baseline shape for conventional detectors with a traditional flow cell.

$$A_{RI} = A_{RI_{static}} + A_{RI_{dynamic}} \quad (9)$$

$$A_{RI} \approx A_{RI_{Fresnel}} + G \cdot \frac{dn}{dt} \quad (10)$$

Ideally  $G = 0$  s and static RI = AU-Fresnel.

The baseline is calculated for the VWD using Eq. (10) and Eq. (3), and compared to the measured data shown in Fig. 4. Of course, the RI as a function of the solvent mixture concentration must be known for the calculation. The G-index determined in  $\Delta n$  experiments is now used to calculate a continuous gradient. Fig. 9 shows the comparison.

The simple model agrees well with the measured data. To apply it, the refractive index as a function of the solvent concentration and temperature is required. The RI data at the correct temperature are not always available, or significant effort is involved in the measurement. The dynamic RI often disturbs more than the static RI component because of abrupt baseline changes. The G-index as a quality measure for the susceptibility to the dynamic RI is easy to measure. In the simplest case, this requires only the measurement of a well-considered sub-step

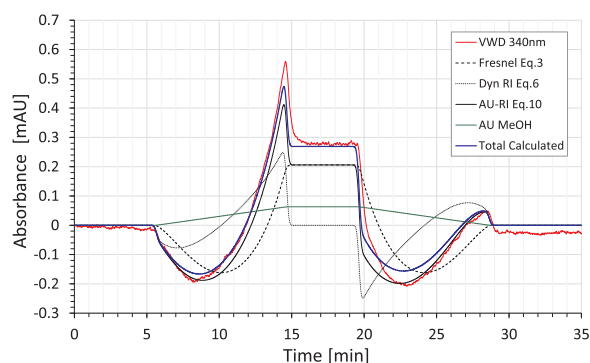


**Fig. 9.** Water-methanol gradient 5%–95%. Red trace: VWD response measured at 340 nm. Black dashed trace: Fresnel losses calculated using Eq. (3) for  $T = +35$  °C. Gray dotted trace: dynamic RI calculated using Eq. (6) with  $G = -2.60$  s. Black trace: apparent absorbance due to RI according to Eq. (10). Green trace: presumed residual background absorbance of methanol 0.07 mAU at 100% methanol at 340 nm. Blue trace: total of all individual calculated components. (For interpretation of the references to color in this figure legend, the reader is referred to the web version of this article.)

of a gradient whose refractive-index difference is known.

The model for the LCW flow cell is different (currently unpublished results of Karsten G. Kraiczek).

## 6. Conclusions

Changes in Fresnel losses due to the changing refractive index (RI) of the mobile phase in gradient elution represent the unavoidable static RI component for the apparent absorbance of a spectrophotometric detector. The Fresnel RI effect can be several tenths of a mAU. Fresnel and other static RI effects originating from the detector and flow cell optics can be easily separated experimentally from dynamic RI effects resulting from changes in the RI of the solvent.

The static RI for a variable-wavelength detector equipped with a conventional cell comes closest to the Fresnel RI effect and shows the same negative curvature. Equally good static RI behavior is achieved for a DAD equipped with an LCW. However, for an LCW, the direction of the static RI changes in sign from positive to negative as the path length increases.

The dynamic RI is superimposed on the static RI and causes abrupt and disturbing baseline changes at the isocratic/gradient and gradient/isocratic transition points. During the gradient, the dynamic RI influences the shape of the baseline.

The G-index as a quality measure for the susceptibility to the dynamic RI is easy to measure. Conventional and LCW cells differ for conceptual reasons in the direction of the dynamic RI effect. However, for the detectability of chromatographic peaks on the baseline, it is not the sign of the G-index that is important but its absolute value. A diode-array detector offers the additional advantage of an optical reference which can compensate to a large extent for dynamic and static RI effects.

## Acknowledgements

Karsten Kraiczek thanks Prof. Sandy Dasgupta (Hamish Small Chair in Ion Analysis, Department of Chemistry and Biochemistry, University of Texas at Arlington) for the stimulating and extremely valuable support during the last several years and for the excellent collaboration as part of the Agilent University Relation program. The authors want to thank Detlev Hadbawnik and Alfred Maute for inspiration and encouragement for this work, also Tom van de Goor and Stefan Schütte for management support at Agilent Technologies.

## Notes

The authors declare no competing financial interest.

## References

- [1] L. Huber, S.A. George (Eds.), *Diode Array Detection in HPLC*, Marcel Dekker, Inc, New York, 1993.
- [2] R. Snyder, J.J. Kirkland, J.W. Dolan, *Introduction to Modern Liquid Chromatography*, Wiley, 2009 (Chapter 4 & 5).
- [3] S. Kromidas, *The HPLC Expert II*, Wiley-VCH, 2017 (Chapter 2).
- [4] D. Guilleme, J. Veuthey, *Guidelines for the use of UHPLC Instruments* ([https://www.hplc.eu/Downloads/UHPLC\\_Guide.pdf](https://www.hplc.eu/Downloads/UHPLC_Guide.pdf)).
- [5] J.N. Little, G.J. Fallick, New considerations in detector-application relationships, *J. Chromatogr.* 112 (1975) 389–397.
- [6] K.E. Nelson, Novel photometric system, U.S. Patent 4,011,451.
- [7] A.C. Gilby, Apparatus and process for measuring light absorbance of fluorescence in liquid samples, US5153679\_A.
- [8] J.E. Stewart, Optics of flow cells for liquid chromatography, *Appl. Opt.* 20 (4) (1981) 654–659.
- [9] C.E. Evans, J.G. Shabushnig, V.L. McGuffin, Experimental and theoretical model of refractive index artifacts in absorbance detection, *J. Chromatogr.* 459 (1988) 119–138.
- [10] C.E. Evans, V.L. McGuffin, Evaluation of refractive index artifacts in liquid chromatography absorbance detection, *J. Chromatogr.* 503 (1990) 127–154.
- [11] G.J.M. Bruin, G. Stegeman, A.C. van Asten, X. Xu, J.C. Kraak, H. Poppe, Optimization and evaluation of the performance of arrangements for UV Detection in high-resolution separations using fused-silica capillaries, *J. Chromatogr.* 559 (1991) 163–181.
- [12] C.N. Renn, R.E. Synovec, Single optical fiber, position-sensitive detector-based multiwavelength absorbance spectrophotometer, *Anal. Chem.* 62 (1990) 558–564.
- [13] S. Jambunathan, P.K. Dasgupta, D.K. Wolcott, G.D. Marshall, D.C. Olson, Optical fiber coupled emitting diode based absorbance detector with a reflective flow cell, *Talanta* 50 (1999) 481–490.
- [14] S.K. Mishra, P.K. Dasgupta, Capillary scale light emitting diode based multi-reflection absorbance detector, *Anal. Chim. Acta* 605 (2007) 166–174.
- [15] K.G. Kraiczek, G.P. Rozing, R. Zengerle, Relation between chromatographic resolution and signal-to-noise ratio in spectrophotometric HPLC detection, *Anal. Chem.* 85 (2013) 4829–4835.
- [16] W. Baumann, Optische Detektoren in der Flüssigkeitschromatographie, *Z. Anal. Chem.* 284 (1977) 31–38.
- [17] T. Dallas, P.K. Dasgupta, Light at the end of the tunnel, *Trends Anal. Chem.* 23 (2004) 385–392.
- [18] J.E. Stewart, Refractive index gradients in stopped-flow and temperature-jump kinetics and liquid chromatography, *Anal. Chem.* 53 (1981) 1125–1128.
- [19] D. Cabooter, F. Lynen, P. Sandra, G. Desmet, Turbulence as a source of excessive baseline noise during high-speed isocratic and gradient separations using absorption detection, *Anal. Chem.* 80 (2008) 1679–1688.
- [20] G. Openheim, E. Grushka, Temperature-dependent refractive index issue using UV-visible detector in high-performance liquid chromatography, *J. Chromatogr. A* 942 (2002) 63.
- [21] E.D. Katz, C.H. Lochmüller, R.P.W. Scott, Methanol-water association and its effect on solute retention in liquid chromatography, *Anal. Chem.* 61 (1989) 349–355.
- [22] P.D.T. Huibers, Models for the wavelength dependence of the index of refraction of water, *Appl. Opt.* 36 (16) (1997) 3785–3787.
- [23] I. Thormählen, J. Straub, U. Griguli, Refractive index of water and its dependence on wavelength, temperature, and density, *J. Phys. Chem.-Ref.-Data* 14 (1985) 933–945.
- [24] Heraeus, *Quartz Glass for Optics, Data and Properties* ([https://www.heraeus.com/media/media/hqs/doc\\_hqs/products\\_and\\_solutions\\_8/optics/Data\\_and\\_Properties\\_Optics\\_fused\\_silica\\_EN.pdf](https://www.heraeus.com/media/media/hqs/doc_hqs/products_and_solutions_8/optics/Data_and_Properties_Optics_fused_silica_EN.pdf)).
- [25] B. Schelle, P. Drefß, H. Franke, K.F. Klein, J. Slupek, Physical characterization of capillary waveguides, *J. Proc. SPIE* 3912 (2000) 150–156.
- [26] K.G. Kraiczek, J. Mannion, S. Post, A. Tsupryk, V. Raghunathan, R. Brennen, R. Zengerle, Micromachined fused silica liquid core waveguide capillary flow cell, *Anal. Chem.* 88 (2016) 1100–1105.
- [27] M.K. Yang, R.H. French, Optical properties of Teflon AF amorphous fluoropolymers, *J. Micro/Nanolithogr. MEMS MOEMS* 7 (3) (2008) 1–9 (033010).
- [28] Agilent 1200 Infinity Series Diode Array Detectors ([https://www.agilent.com/cs/library/usermanuals/public/G4212-90013\\_DAD-A-B\\_USR\\_EN.pdf](https://www.agilent.com/cs/library/usermanuals/public/G4212-90013_DAD-A-B_USR_EN.pdf)).
- [29] S.R. Bakalyar, M.P.T. Bradley, R. Honganen, The role of dissolved gases in high-performance liquid chromatography, *J. Chromatogr.* 158 (1978) 277–293.
- [30] J.N. Brown, M. Hewins, J.H.M. van der Linden, R.J. Lynch, Solvent degassing and other factors affecting liquid chromatographic detector stability, *J. Chromatogr.* 204 (1981) 115–122.
- [31] R. Battino, T.R. Rettich, T. Tominaga, The solubility of oxygen and ozone in liquids, *J. Phys. Chem. Ref. Data* 12 (2) (1983) 163–177.